Aerodynamic and Aeroacoustic Measurements of a Landing Gear Torque Link

Sarah Windiate*, Oksana Stalnov†, David Angland‡, and Xin Zhang§
University of Southampton, Southampton, Hampshire, SO17 1BJ, UK
Richard Ashworth¶
EADS Innovation Works UK, Bristol, BS99 7AR, UK

Aerodynamic and aeroacoustic measurements were performed on a $1/3^{\text{rd}}$-scale landing gear torque link model, comprised of a generic strut and torque link. The objective was to provide an aerodynamic and aeroacoustic experimental database for CFD validation for a torque link with varying torque angle and yaw angle, with the future objective being noise attenuation. Torque link angles of $\theta = 90^\circ$, 110° and 130° and yaw angles of $0^\circ \leq \phi \leq 180^\circ$ were tested. The Reynolds number ranged from $6.5 \times 10^4 \leq Re \leq 2.7 \times 10^5$, based on the strut diameter. A torque link angle of $\theta = 130^\circ$ resulted in the strut and torque link behaving as a single bluff body with reduced drag and suppressed vortex shedding from the strut. However, no discernable decreases in local noise source levels were recorded for varying the torque link angle. Increasing the yaw angle from $\phi = 0^\circ$ resulted in several different flow regimes, with a suppression in vortex shedding for $90^\circ \leq \phi \leq 150^\circ$. At 2 kHz, phased microphone array measurements showed interaction noise to dominate any additional noise caused by extending the torque arms into the freestream. At the optimal yaw angle of $\phi = 90^\circ$, drag levels were 72% higher than the baseline case of $\phi = 0^\circ$ and local noise source levels were lower over the 2 kHz $\leq f \leq$ 8 kHz frequency range.

Nomenclature

C_D	Coefficient of drag
C_L	Coefficient of lift
D	Strut diameter (m)
f	Frequency (Hz)
L	Strut length (m)
p_{ref}	Reference pressure (Pa)
Re	Reynolds number based on cylinder diameter
St	Strouhal number based on cylinder diameter
U'	Root-mean-squared velocity (m/s)
$\overline{U}$	Mean streamwise velocity (m/s)
U_∞	Freestream velocity (m/s)
x, y, z	Co-ordinate axis (m)

Greek Symbols

θ	Torque link angle (degrees)
ϕ	Yaw angle (degrees)

*EngD Student, Faculty of Engineering and the Environment, Student Member AIAA.
†Research Fellow, Faculty of Engineering and the Environment, Member AIAA.
‡Lecturer, Faculty of Engineering and the Environment, Member AIAA.
§Airbus Professor of Aircraft Engineering, Faculty of Engineering and the Environment, Associate Fellow AIAA.
¶Research Engineer, TCC3 Aeromechanics.

Abbreviations

CCD	Charge-coupled device
CFD	Computational fluid dynamics
FFT	Fast Fourier transform
OASPL	Overall sound pressure level (dB)
PIV	Particle image velocimetry
PSD	Power spectral density (dB / Hz)
rms	Root-mean-square
SPL	Sound pressure level (dB)

I. Introduction

Aircraft noise regulations are becoming increasingly stringent, with the Advisory Council for Aerospace Research in Europe (ACARE) setting a target for a 50% reduction, based on a 2000 baseline, in perceived external noise from aircraft by 2020.[1] In order to meet targets such as this, all aspects of aircraft noise are being researched simultaneously, including the landing gear which is widely considered to be the dominant source of airframe noise on most large modern aircraft. Studies conducted in the early 1970s by Heller and Dobrzynski[2] showed that high lift devices and deployed landing gears resulted in noise levels that were 10 dB higher than for an aircraft in the clean cruise configuration.[3] Subsequent work performed by Airbus confirmed that landing gears are the dominant noise source for large capacity aircraft in the landing approach phase[3,4] which will become an increasing problem as aircraft becomes larger and noise regulations become more stringent.

Landing gears are extremely complex structures comprising numerous bluff bodies, which generate aerodynamic noise through flow separation and the interaction of turbulent wakes with downstream components. Therefore the modelling of landing gear noise requires an understanding of flow interactions between different components.[5] This study focuses on the torque link, which is a 'scissor-like' component normally positioned downstream of the main landing gear strut. The torque link serves the purpose of keeping the lower strut aligned with both the upper strut and the rest of the aircraft. As they are designed for ease of inspection and maintenance, torque links are therefore considered a non-aerodynamic structure.[6] Investigations into the aerodynamic and aeroacoustic traits of the landing gear torque link include the work of Huang et al.[7–9] who used plasma actuators to research broadband flow-induced noise control. The noise control effects of plasma actuators were investigated in the University of Southampton's anechoic chamber, using a 25% scale model of a generic main strut and torque link. A microphone arc and phased microphone array were used to collect acoustic data. Data was collected using both upward and downward directed actuation, with results highlighting that upstream directed actuation performed more effectively. Upstream actuation was shown to attenuate noise effectively in the 1 kHz - 3 kHz frequency range. However, noise control effectiveness was reduced with higher frequencies due to interference from the self noise of plasma actuators. Actuation was found to be successful in reducing the overall sound pressure level (OASPL) emanating from the configuration by up to 3.2 dB, whereas beamforming showed a 3 dB reduction at frequencies of interest.

Despite the work of Huang et al. there are few investigations into the aerodynamic and aeroacoustic characteristics of the landing gear torque link. Instead there are various mentions in literature of the torque link as a noise source as part of whole landing gear simulations or experimental studies. One such study is that of Jaeger et al.,[6] who conducted an experiment on an isolated 26% scale Boeing 777 high fidelity 6-wheel landing gear in the NASA Ames 7 × 10 foot, hard-wall closed circuit wind tunnel. The torque link was identified as a major noise source from sideline tests, it was found that the torque link contributes up to 8 dB (integrated sound pressure level (SPL)) to sideline noise at 900 Hz. In terms of noise abatement methods, Jaeger et al. state that of all landing gear structures, the torque link may be the least amenable to major modification since its operation dictates its profile, therefore only minor cosmetic alterations may be feasible. A similar experiment to Jaeger et al., was undertaken by Ravetta et al.[10] who utilised the same 26% scale Boeing 777 main landing gear model. The experiments were performed in the Virginia Tech stability wind tunnel. Ravetta et al. tested 15 different configurations at flyover and sideline positions. They found the torque link to be one of the dominant noise sources at 2 - 3 kHz in the sideline position. This result is corroborated by Guo[11] who compared an empirical model to experimental data obtained by Stoker.[12] Guo concluded that noise data from a Boeing 737 main landing gear was dominated in the range 800 Hz - 1 kHz by a tone caused by vortex shedding from the torque link, however this proved to be specific to the

experiment only and was not observed in Guo's other measurements.

In terms of the torque link as a noise generating source, literature suggests that the main sources of noise for a torque link are caused by the flow separation and wake interaction between the torque link and the main strut. Dobrzynski et al.[13] simulated various landing gear configurations for the sole purpose of designing a low-noise gear, configurations included a re-designed A340 nose landing gear. Dobrzynski et al. found the wake from the strut to impinge upon the downstream torque link. As this is considered detrimental, the torque link was moved upstream of the strut and the flow characteristics for this configuration showed no apparent interaction noise. A comparison between experimental data from NASA for a 25% scale Gulfstream G550 nose landing gear was performed by Zawodny et al.[14] In terms of acoustic data, the dominant noise sources were found to be the wheels ($f = 1.25$ kHz), the torque arms ($f = 2.5$ kHz) and the light cluster ($4 \leq f \leq 8$ kHz). Neuhart et al.[15] further examined the experimental data and found the wake from the strut impinging upon the torque arms to be symmetric and devoid of any large scale vortical structures. Thus, the proximity of the torque arms to the strut acts to suppress periodic shedding from the strut.[15]

One problem inherent with the identification and classification of noise generated by the torque link from whole landing gear investigations is that it can be difficult to extract information solely about the torque link due to the effects of the wheels and other components influencing the flowfield. Therefore, this study identifies the noise generating sources of the torque link and the interaction of flow between the strut and torque link by testing these components in isolation i.e. a strut and torque link configuration. Both aerodynamic and aeroacoustic measurements have not been previously conducted on a landing gear and torque link configuration to this degree, therefore this investigation offers a novel approach to airframe noise research. This study is separated into two investigations, firstly the effect of altering the torque link angle θ, and secondly the effect of yaw angle ϕ, as shown in Figure 1. The importance of the torque link and yaw angles is discussed in the following section.

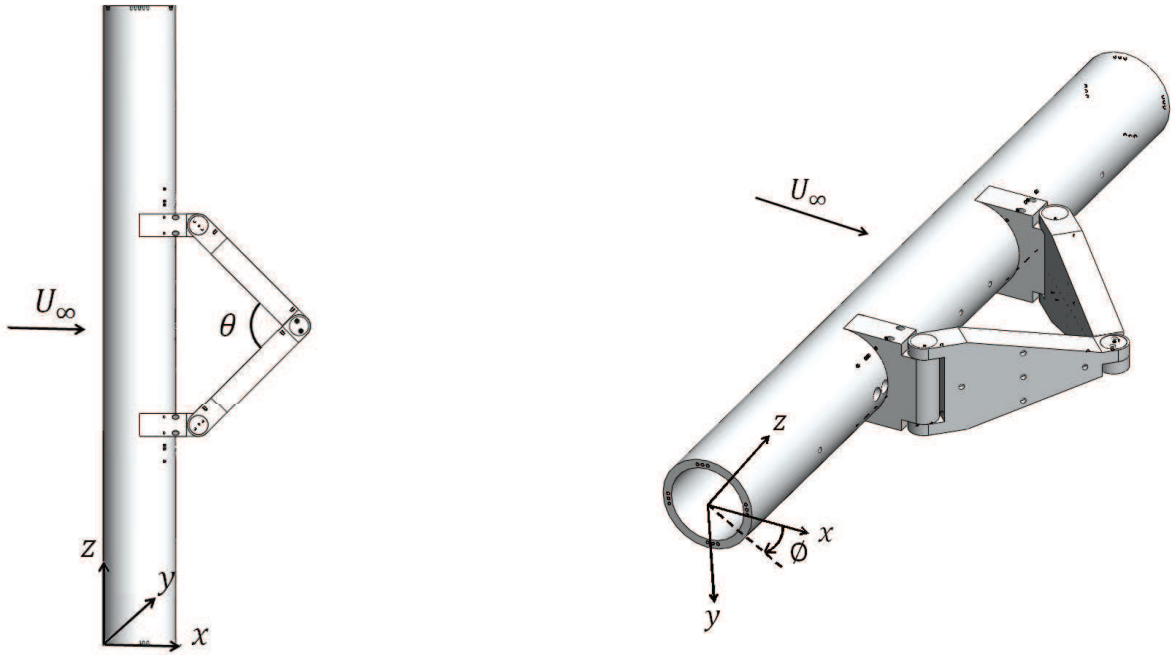

(a) Definition of torque link angle θ.

(b) Definition of yaw angle ϕ.

Figure 1. Definition of torque link angle and yaw angle.

II. Experimental Apparatus

A. Model Design

A generic landing gear strut and torque arms were designed from an Airbus A340 landing gear, the model was scaled to $1/3^{\text{rd}}$. The torque arms were heavily simplified to allow for future CFD meshing. The torque arm

bracket was designed to affix straight to the strut instead of encircling the strut - this ensured the bracket did not protrude beyond the surface of the strut so all noise was caused by interaction between the strut wake and torque arms. The strut measured $L = 0.9$ m in length and $D = 0.1016$ m in diameter, giving an aspect ratio of $L/D = 9$. Furthermore, the strut was fitted between two rectangular end plates $8D$ in width and $7D$ in height, with the distance between the strut axis and the leading edge being $3.5D$. Leading edge separation of the boundary layer from the end plates was controlled by fitting a small flap to the trailing edge of each plate. When the model was placed inside the University of Southampton's 2.1 m $\times$ 1.5 m wind tunnel it had a test-section blockage ratio of 2.8%. In order to achieve the correct supercritical flow regime experienced in the landing approach phase, the strut was tripped to turbulence using carborundum grit which had an average particle size of 2.7 x 10^{-4} m (Grit 60). A short study was performed on the location of the transition strips. A location of $\pm 50^\circ$ from the stagnation point was considered optimal and the transition strips, 11.8 mm in width, were placed along the length of the strut at this position.

1. Torque Link Angle

When the strut and torque arm junction are considered in isolation to be tandem cylinders then one can apply the critical spacing laws of Igarashi[16] and Zdravkovich.[17] These laws state that for critical spacing values less than $1.1D$ then tandem cylinders behave as a single bluff body. Therefore, an investigation was conducted to determine whether critical spacing values less than $1.1D$ for the strut and torque link resulted in the entire configuration behaving as a single bluff body i.e. no flow reattachment from the strut onto the downstream torque arms. This would result in less noise due to flow interactions between the strut and torque link. Furthermore, Neuhart et al.[15] suggested that the proximity of the torque arm to the strut acts to suppress periodic vortex shedding from the strut. Therefore by increasing the angle of the torque arms they are in effect moving closer to the strut which may act to suppress periodic vortex shedding and affect the noise levels of the whole configuration. A separation distance of $1.1D$ corresponded to a torque angle of $\theta = 110^\circ$. Three different angles were tested, $\theta = 90^\circ$ was tested as the 'baseline' configuration and offered as a comparison to all other configurations. A torque link angle of $\theta = 110^\circ$ was tested as this angle is on the threshold of the separation distance. In theory this configuration should behave as a single bluff body but due to the complex three-dimensional nature of the configuration this may not be the case. Lastly, a torque link angle of $\theta = 130^\circ$ was tested as this angle is significantly larger than the separation threshold.

2. Yaw Angle

The model has been designed so that the entire configuration can be rotated to investigate yaw angles from $0^\circ \leq \phi \leq 180^\circ$, in 15° increments, where $\phi = 180^\circ$ corresponds to the torque arms placed upstream of the strut. It is important to model the effects of cross flow since a landing gear can experience cross-winds during the landing approach phase. By rotating the configuration, the torque arms are moved from directly behind the strut to directly upstream. Therefore, during this rotation the flow physics behind the configuration will alter. The torque arms will no longer sit in the region behind the strut and this will lessen impingement of the strut's wake onto the torque arms. One counter-effect of this lessened impingement is that the torque arms will extend further into the free-stream and therefore, will cause increased drag (which is a desirable effect in the landing approach phase), but this may also cause additional noise.

B. Wind Tunnel

All experiments were performed in the high speed section of the University of Southampton's 2.1 m $\times$ 1.5 m wind tunnel. The wind tunnel is a closed circuit tunnel and has a working section length of 4.4 m. Wind speeds ranging from 4 m/s to 45 m/s can be tested, with the incoming turbulence intensity being approximately 0.3% at 45 m/s.[18]

C. Force Measurements

Forces were collected using a weigh-beam balance which allows for time-averaged forces to be collected. Drag forces were measured over a period of 15 seconds. Furthermore, the short-term repeatability error was less than 1%, whereas the long-term repeatability error was less than 5%. Forces were collected at several Reynolds numbers for each configuration. The final force data was extracted by subtracting the tare value (endplates and ceiling struts only) from the given force data at each Reynolds number.

D. On-Surface Microphones

The microphones used for the on-surface pressure measurements were 6 mm Panasonic WM-61A omnidirectional condenser microphone cartridges, which were mounted flush within the surface of the model. The model featured five on-surface microphones, three of which were situated in between the torque arms. The nominal sensitivity of the microphones was -35 dB ± 4 dB (using reference pressure $P_{ref} = 2 \times 10^{-5}$ Pa), with a frequency range of 20 Hz to 20 kHz. The signal-to-noise ratio was more than 62 dB. The signal from the microphones was sampled at 48 kHz, and acquired using a National Instruments PXI-4472 data acquisition card. A total of 100 blocks, each containing 4096 samples, were taken for each configuration. These were then analysed using a Fast Fourier Transform (FFT) to compute the power spectral density. Only microphones 1 - 3 are presented in this study, 4 and 5 are omitted due to their similarities with microphones 1 and 2.

E. Particle Image Velocimetry

A TSI Insight 4G system was used to both capture and to post-process the PIV data. The air was seeded with particles using a smoke generator placed downstream of the model inside the wind tunnel, thus ensuring that the smoke had diffused sufficiently for PIV purposes by the time it reached the test section. Two pulsed Nd:YAG (yttrium aluminum garnet) lasers operating at 3.63 Hz, situated in the wind tunnel, were used to illuminate the particles. The laser sheet was emitted in both a horizontal ($x - z$ plane) and vertical plane ($x - y$ plane) approximately 3 mm thick. Digital images were captured by a Kodak CCD (charge-coupled device) camera using a Nikon 60 mm lens. A TSI synchronizer box controlled the firing of the lasers and the timing of the camera. Two digital images were captured 20 - 30 μs apart, depending on the configuration and wind speed. The data was pre-processed during analysis, which acted to remove 'background' light and thus render the smoke particles more visible and easier to process. During processing a recursive Nyquist grid was used with a 50% grid spacing overlap for an interrogation area measuring 32 × 32 pixels. A peak validation value of 1.1 was used to reject spurious vectors. The data was then averaged over 500 images to obtain the mean velocity magnitude and root-mean-squared velocity components.

F. Microphone Array

A 112 channel microphone array was used to aid localisation of the noise sources. The array was used to yield information by beamforming, therefore a qualitative data set was obtained but accurate absolute levels were not achievable due to reflection from the wind tunnel walls. When collecting acoustic data in a wind tunnel one needs to be aware of the turbulent boundary layer noise over the microphone array, high background noise levels generated by the fan and flow over the wind tunnel and lastly, the hard walls giving rise to additional noise sources.[19]

The microphone array featured 112 microphones situated 12.7 mm behind an acoustically transparent cloth. The microphones used were 6 mm Panasonic WM-61A omni-directional electret condenser cartridges, as previously described. The array was placed on the floor of the wind tunnel, approximately 0.73 m below the centreline of the model. The phased microphone array data was acquired using a National Instruments PXI-4472 data acquisition card connected to a pre-amplifier. The sampling frequency was set at 48 kHz, the block size was 4096 and the data was averaged over 100 blocks. The signals collected from the microphone array were corrected for magnitude and phase, using previous calibration files. The data was then post-processed with an in-house beamforming code.[19]

III. Results and Discussion

A. Effect of Torque Link Angle

1. Aerodynamic measurements

The time averaged drag coefficients C_D for the strut only and the three configurations with varying torque angle θ are presented in Table 1 for $Re = 2.7 \times 10^5$. The values were normalised using the frontal area of the strut, corresponding to 0.09 m^2. In terms of corroborating the experimental data, the drag coefficient for the strut sits within the range of drag coefficients recorded in literature at this Reynolds number.[20] By affixing the torque link to the strut with $\theta = 90°$, $\phi = 0°$, the C_D is lower than that of the strut only.

This suggests that the torque arms act to suppress strong vortex shedding from the strut thereby reducing the drag coefficient. Increasing the torque link angle θ to 110° and 130° acts to further reduce the drag. Therefore by increasing the torque link angle, the distance between the torque arm junction and the strut is decreased, thereby allowing the entire configuration to behave as a single bluff-body.

A Reynolds number dependence study was performed to evaluate the effect of the transition strips. Drag coefficients were collected for tripped (Grit60) and non-tripped (clean) configurations, as presented in Figure 2. This figure shows the non-tripped data remaining fairly constant over the Re range, this is because the cylinder experiences no transition to turbulence so is effectively at a much lower Re, i.e. the subcritical range according to Achenbach's[21] curve representing Re as a function of C_D. The tripped data shows different behaviour over the range of Re, the large drop in C_D at approximately $Re = 0.8 \times 10^5$ suggests transition to the critical regime. Therefore, the act of tripping the cylinder serves to move the C_D regime of the configuration from the subcritical regime into the supercritical regime.

Configuration	C_D
Strut only	0.542
Strut with torque arms, θ=90°, ϕ=0°	0.522
Strut with torque arms, θ=110°, ϕ=0°	0.521
Strut with torque arms, θ=130°, ϕ=0°	0.504

Table 1. Drag coefficient of configurations with varying torque link angle at $Re = 2.7 \times 10^5$.

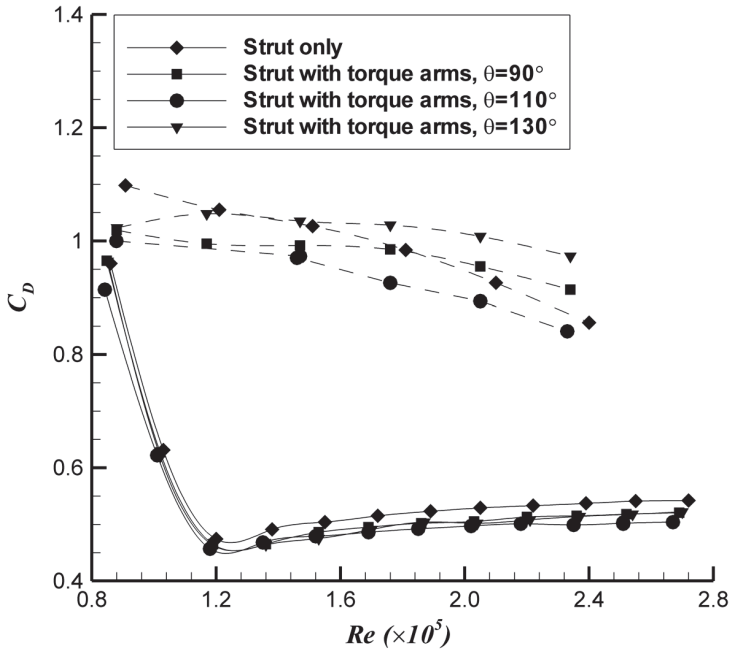

Figure 2. Reynolds dependence study for configurations with varying torque link angle, yaw angle $\phi = 0°$ (dotted lines are clean, solid lines are tripped).

The mean streamwise velocity and root-mean-squared velocity for the strut only case and the three configurations with varying torque link angle are presented in Figures 3 and 4. The reflections from the PIV system and the torque link are shaded in black, and the cylinder is shaded white. Only the u' component is plotted for the root-mean-squared velocity as this component showed greater fluctuations than v'. The mean streamwise velocity for the strut only case, Figure 3(a), shows that the recirculation region extends

$1.8D$ downstream of the strut. Separation is seen to occur at approximately $\pm$ 100° from the stagnation point which leads to a narrow wake approximately $0.5D$ wide, $1.5D$ downstream. When the torque arms are added, separation is seen to occur on the torque arms at the point where they taper down to the torque arm junction, at approximately $x/D = 1.4$. A short recirculation region extends from the end of the torque arms, approximately $0.3D$ in length. Separation is seen to occur at the same point when the torque link angle is increased from $\theta = 90°$ to $\theta = 110°$ and 130°. The wake for $\theta = 130°$ is shown to rapidly narrow after separation. This is possibly due to the sharper angle of separation than the $\theta = 90°$ and $\theta = 110°$ configurations. The rms velocity shows the streamwise velocity fluctuations in the shear layers. There are two strong regions of increased fluctuations which correspond to vortex shedding for the strut only, as shown by the streamlines overlaid. By affixing the torque arms, these strong fluctuations are almost entirely suppressed, as shown by the absence of coherent strong vortices emanating from the strut. Instead there are two smaller and weaker lobes of fluctuations emanating from the points of separation on the torque arms. Furthermore, these regions of fluctuations are shown to be weaker for $\theta = 110°$ and 130° than for $\theta = 90°$, suggesting a more stable flow regime for these configurations.

When the torque link angle is increased to $\theta = 110°$, the torque arms extend approximately $2D$ downstream of the strut, therefore extending further than the recirculation region of the strut only case. As the torque link extends further than this recirculation region, parts of it extend into the freestream, such as the corners of the torque arm junction. These parts may cause additional noise due to the higher oncoming velocity. However, when the torque angle is increased to $\theta = 130°$, the footprint of the configuration fits within the recirculation region of the strut only case. This suggests that this configuration may record lower noise levels than torque link angles of $\theta = 90°$ and 110° and the strut only case.

The momentum deficits for the three configurations with varying torque link angle θ are plotted in Figure 5(a) for a wake profile taken along $x/D = 2.7$. The momentum deficit was calculated by integrating the normalised mean streamwise velocity over the PIV window. The corresponding wake profiles are plotted in Figure 5(b), with comparison to the strut only case. Figure 5(a) shows that by increasing the torque link angle the momentum deficit decreases, thereby suggesting that the torque link angles of $\theta = 110°$ and 130° have narrower and shorter wakes than $\theta = 90°$. This is supported by Figure 5(b) which shows $\theta = 130°$, in particular, to have a much narrower and shorter wake than all other configurations, including the strut only case.

2. On-Surface Pressure Fluctuations and Noise Sources

Noise spectra for the on-surface microphones are plotted as power spectral density (PSD) in Figure 6 using equation (1), where $p(t)$ is the pressure signal measured, $n = 4096$ is the number of samples per block, $F_s =$ 48 kHz is the sampling frequency and the reference pressure is $P_{ref} = 2 \times 10^{-5}$ Pa. The power spectra of the pressure signals were calculated with a frequency resolution of 11.7 Hz. No windowing function was used. Three datasets were collected to determine short-term repeatability. All microphones recorded a weak tonal peak at $St = 0.5$ for the strut only. This corresponds to shedding from the strut at a Strouhal number of 0.25 as the microphones are on the centreline aligned with the drag dipole, therefore recording a doubling of the frequency. Microphone 1 shows that affixing the torque arms to the strut causes a local decrease in on-surface pressure fluctuations corresponding to approximately 5 dB from $0.1 \leq St \leq 10$. Furthermore, the tonal peak is suppressed by the presence of the torque arms. It can be seen that the addition of the torque arms interrupt shedding from the strut, thereby reducing the noise. Despite the reduction in noise by attaching the torque arms, there was little effect of varying the torque link angle for microphone 1. Microphone 2 shows opposing behaviour to microphone 1, displaying a local increase in noise caused by the addition of the torque arms. This increase in local pressure fluctuations may be attributed to the proximity of the torque arms to the microphone, for example, the loudest configurations are for $\theta = 110°$ and 130° which is where the torque arms move closer to the strut and thus move closer to the microphones. Microphone 3 shows that a torque link angle of θ=130° records the lowest local pressure fluctuations of all configurations, even lower than the strut only, which further confirms that by increasing the torque link angle, the torque arms act to suppress vortex shedding and the entire configuration acts as a single bluff body. Microphone 3 also shows that torque link angles of $\theta = 90°$ and 110° record higher local noise levels than the strut only case. This extra noise may be attributed to the torque arm junction extending out of the struts recirculation region into the freestream and therefore acting as an additional local noise source.

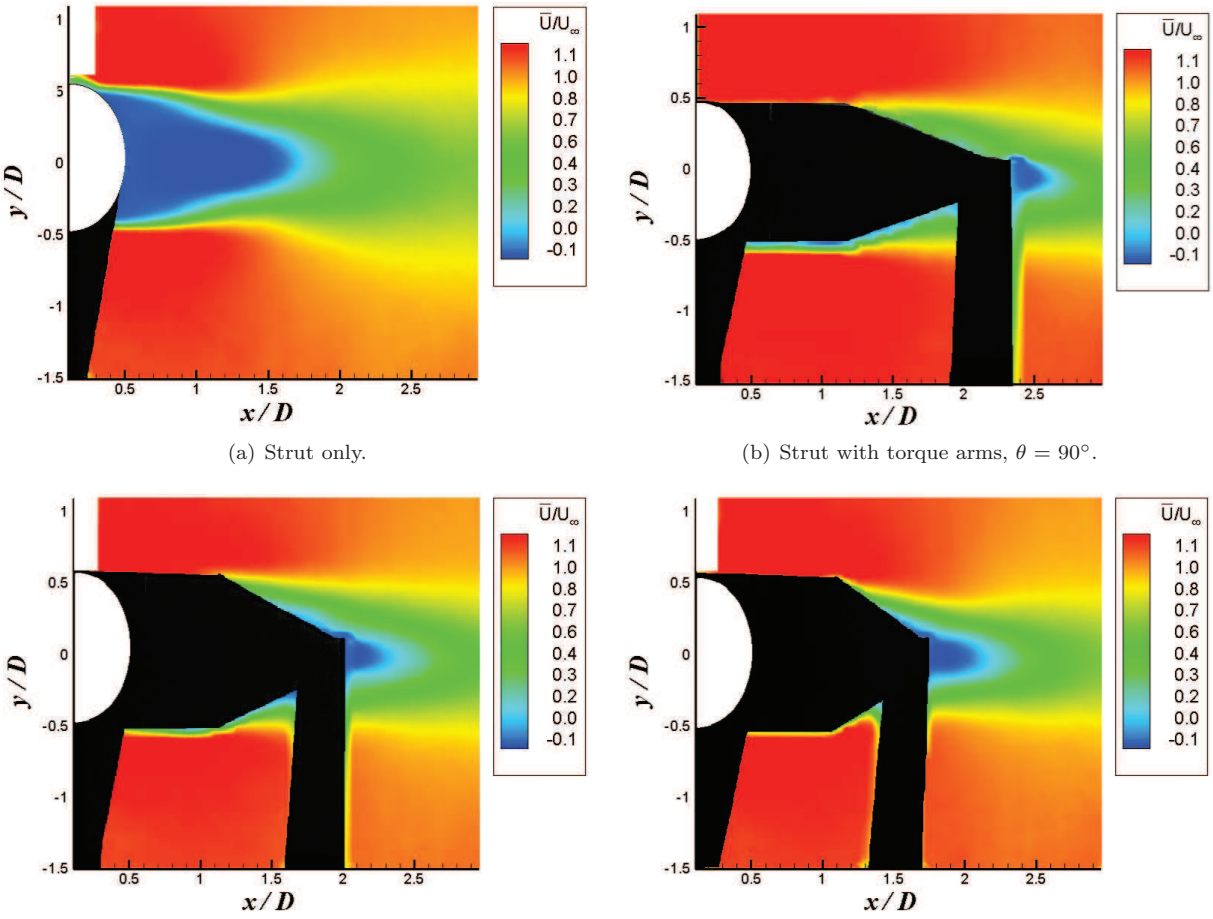

(a) Strut only.

(b) Strut with torque arms, $\theta = 90°$.

(c) Strut with torque arms, $\theta = 110°$.

(d) Strut with torque arms, $\theta = 130°$.

Figure 3. Mean streamwise velocity for strut only and configurations with varying torque link angle, yaw angle $\phi = 0°$, $z/D = 4.5$.

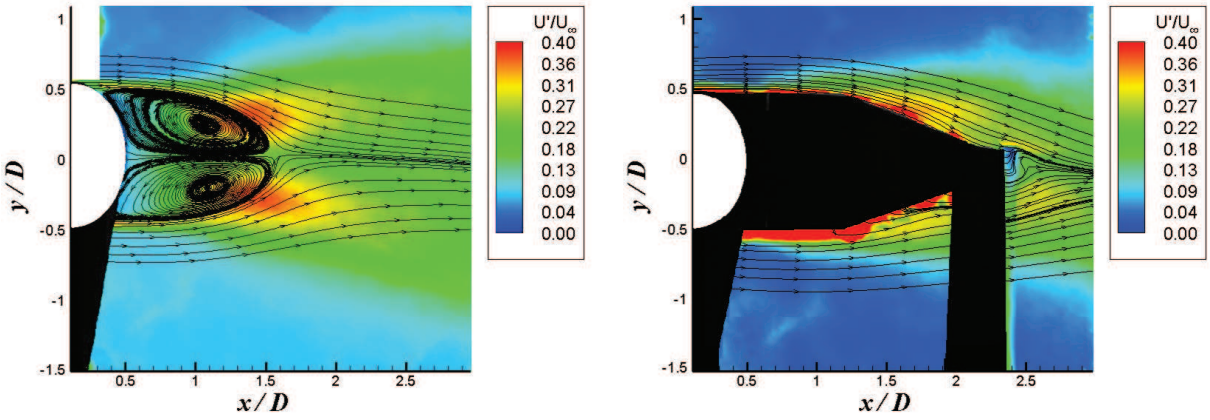

(a) Strut only.

(b) Strut with torque arms, $\theta = 90°$.

(c) Strut with torque arms, $\theta = 110°$.

(d) Strut with torque arms, $\theta = 130°$.

Figure 4. Root-mean-squared velocity with streamlines for strut only and configurations with varying torque link angle, yaw angle $\phi = 0°$, $z/D = 4.5$.

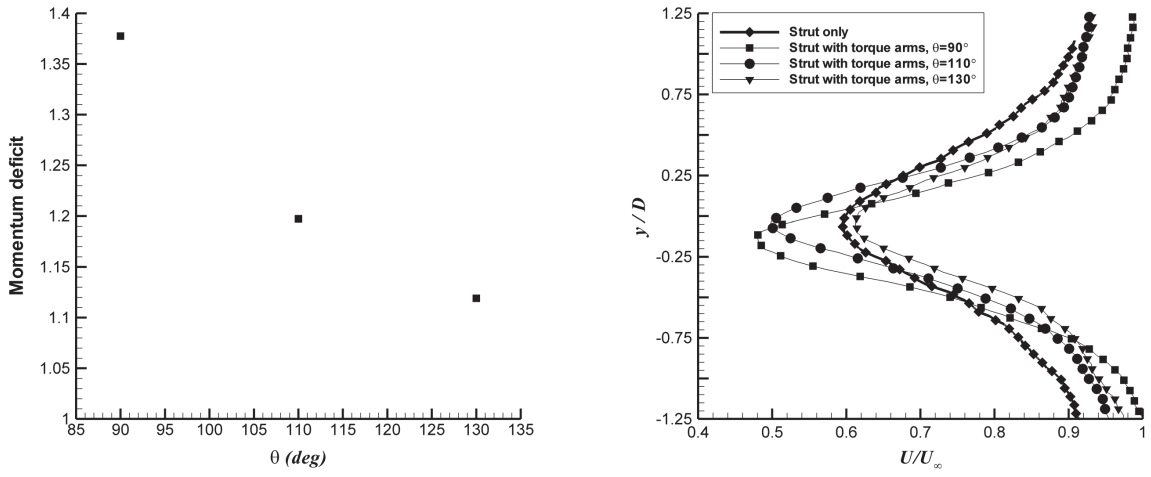

(a) Momentum deficit.

(b) Wake profiles.

Figure 5. Momentum deficit and wake profiles along $x/D = 2.7$ for strut only and configurations with varying torque angle, yaw angle $\phi = 0°$.

$$P(\omega) = \frac{2 \mid \mathrm{FFT}(p(t)) \mid^2}{n \cdot F_s} \tag{1}$$
$$\mathrm{PSD}(\omega) = 10\log_{10}\frac{P(\omega)}{{P_{ref}}^2}$$

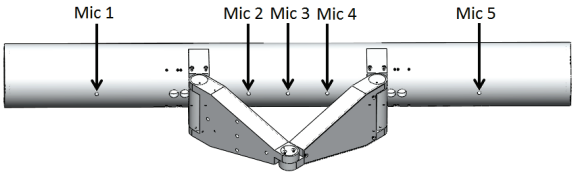

(a) Microphone locations.

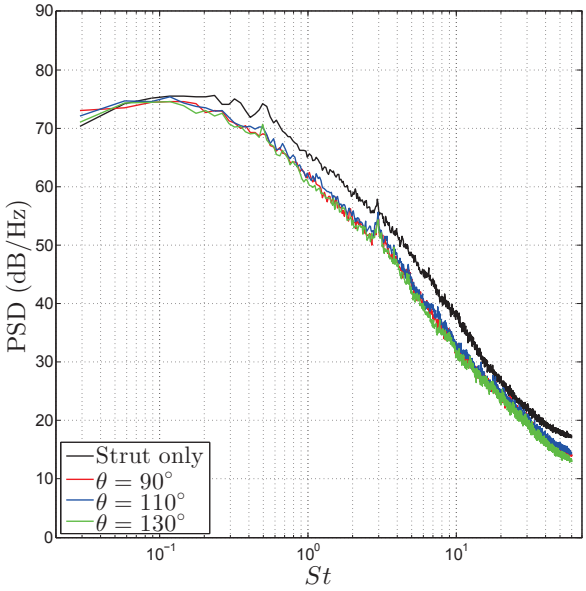

(b) Microphone 1.

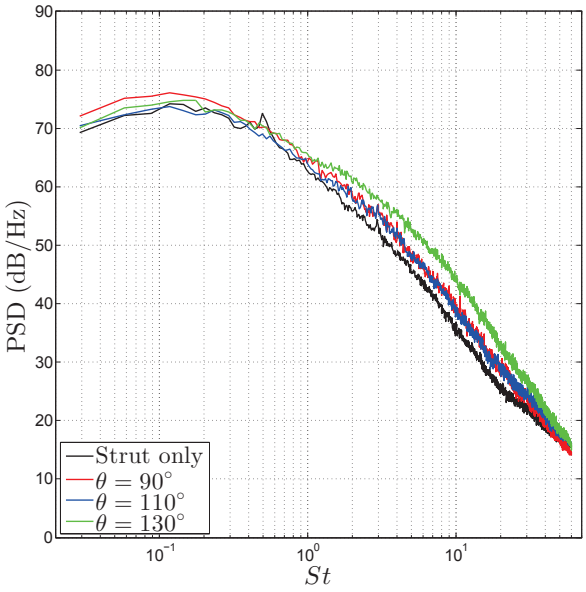

(c) Microphone 2.

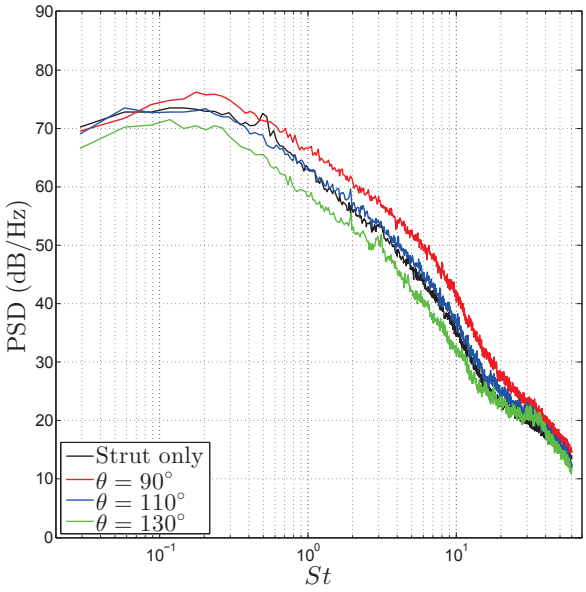

(d) Microphone 3.

Figure 6. PSD for varying torque link angle.

Phased microphone array plots were integrated over 2 kHz $\leq f \leq$ 8 kHz and are presented in Figure 7 for OASPL (dB) and SPL (dB) over the whole frequency range. No discernable differences in integrated SPL are recorded for the three configurations with varying torque link angle, despite having notable differences in the aerodynamic measurements. Figure 7(b) shows the strut only case to be approximately 1 dB quieter than all

other configurations over $2.5 \leq f \leq 8$ kHz. This difference is reduced at 2 kHz, suggesting that the noise due to the strut only dominates at this particular frequency. Therefore, the torque arms are shown to contribute an extra 1 dB to nearfield noise sources in this frequency range. The SPL profiles for each configuration are all shown to decrease over the measured frequency range, this is due to the model featuring no small scale detail, therefore the overall nearfield noise levels feature little high frequency content.[11] Instead the SPL profiles record the greatest levels over the mid frequency range of 2 kHz $\leq f \leq$ 2.5 kHz due to the length scale of the strut being relatively large.

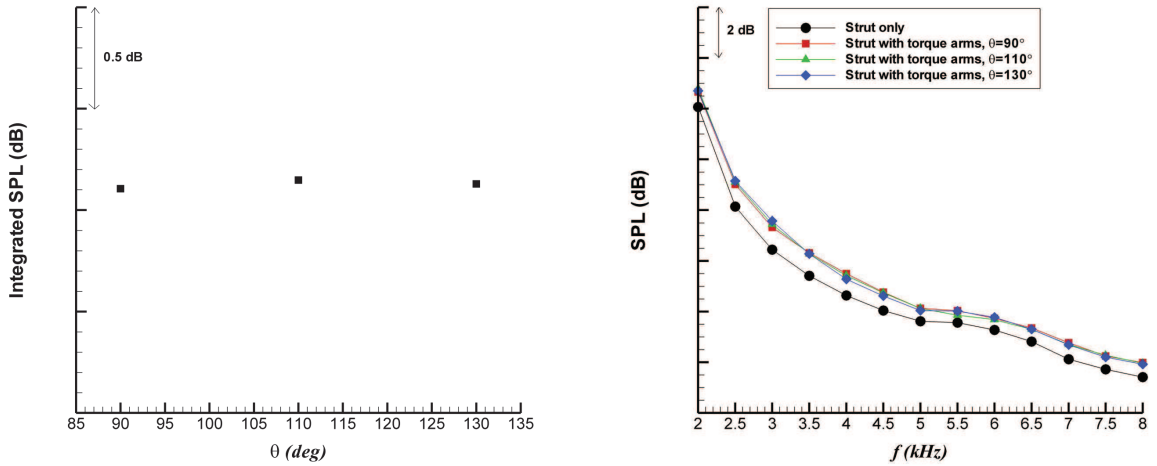

(a) Integrated SPL (dB).

(b) SPL (dB).

Figure 7. Beamforming maps integrated over 2 kHz $\leq f \leq$ 8 kHz for varying torque link angles, yaw angle ϕ = 0°.

B. Effect of Yaw Angle

1. *Aerodynamic measurements*

Drag coefficients were collected for each configuration, with C_D plotted against yaw angle ϕ for $Re = 2.7 \times 10^5$ in Figure 8. The largest value of drag is recorded at $\phi = 75°$ as this configuration has a large frontal area in contact with the free-stream. It is also shown that the baseline case, $\phi = 0°$ exhibits the lowest level of drag as the torque arms are sitting directly downstream of the strut. Therefore, the addition of torque arms onto the strut acts to suppress vortex shedding from the strut, resulting in decreased levels of drag. When the torque arms are upstream of the strut, $\phi = 180°$, the drag exhibited is 51% larger than the baseline case therefore demonstrating that the torque arms to not shield the strut as well as the reverse case. However, additional drag is considered beneficial during the landing approach phase.

The mean streamwise velocity component for different yaw angles is presented in Figure 9. Several yaw angles are omitted due to their similarities to other angles, however, these angles are mentioned below to describe distinct flow regimes. By rotating the model to $\phi = 15°$ a much wider wake is generated than the baseline case of $\phi = 0°$. At this angle separation is seen to occur firstly from the torque arm / strut region, and secondly near to the end of the torque arm. At $\phi = 45°$, the flow is seen to pass through the torque arm 'gap region'.

From $30° \leq \phi \leq 90°$ there are two distinct wakes, one from the strut and one from the junction where the torque arms join, as shown for $\phi = 45°$. Both wakes are angled upwards due to flow passing through the gap region. Another regime is present from $105° \leq \phi \leq 135°$ when the torque arms are situated upstream of the strut. These angles show extended wakes potentially due to the bracket connecting the torque arms to the strut extending into the freestream. By rotating the configuration further to $\phi = 150°$ the torque arms are almost in line with the strut resulting in a shorter wake. At $\phi = 180°$ there is a truncated and narrower wake than is seen at all other configurations, even the strut only case. There is a faster recovery to the freestream for $\phi = 180°$ than the strut only case with reduced velocity fluctuations present in the

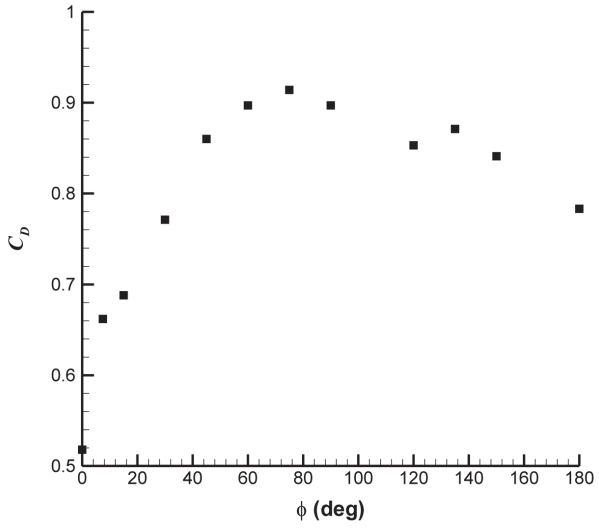

Figure 8. C_D for configurations with varying yaw angle, torque link angle $\theta = 90°$.

wake. Figure 10 presents the velocity fluctuations with streamlines overlaid. These streamlines show a much shorter, narrower vortex formation behind $\phi = 180°$ than is seen in the strut only case, which suggests that affixing the torque arms upstream of the strut acts to interrupt strong periodic shedding from the strut with shorter, weaker vortices emanating from the configuration.

Streamlines show relatively small velocity fluctuations behind the torque arms for $\phi = 0°$. By 7.5° there are two distinct regions of increased velocity fluctuations, the first corresponds to the separation of flow from the torque arm / strut region. The second region is located near to the end of the torque arms, and is angled upwards due to flow passing through the gap region. These two regions of increased fluctuations are also present for $\phi = 45°$, however, the location of the region near to the end of the torque arms has moved due to the rotation of the torque arms. At $\phi = 90°$ the levels of velocity fluctuations are reduced. There are now two regions of fluctuations corresponding to flow separation from the strut. These regions become elongated at $\phi = 135°$ due to the bracket connecting the torque arms to the strut extending into the freestream. At $\phi = 180°$ the bracket is directly upstream of the strut, therefore the two regions of fluctuations are much reduced in size. The regions of increased velocity fluctuations for the strut only, as shown in Figure 4, extend further than those exhibited by $\phi = 180°$. Thus further suggesting that the presence of the torque arms upstream of the strut acts to suppress strong periodic vortex shedding from the strut with the resulting vortex shedding from $\phi = 180°$ having a shorter vortex length.

Notable wake profiles are plotted in Figure 11, several profiles have been omitted to maintain clarity. The momentum deficit is shown to greatly vary with yaw angle ϕ. The baseline case of $\phi = 0°$ has a relatively small momentum deficit compared to yaw angles of $7.5° \leq \phi \leq 75°$, as shown by $\phi = 15°$ in Figure 11. This is due to the extremely wide wakes that emanate from yaw angles of $7.5° \leq \phi \leq 15°$ and the combined momentum deficit from the two separate wakes that emanate from the strut and torque arms for yaw angles of $30° \leq \phi \leq 75°$. Other notable conclusions include $\phi = 180°$ recording a lower momentum deficit than the baseline case of $\phi = 0°$. This is evident in both the mean streamwise velocity plots and the wake profiles in Figure 11(b), which highlights $\phi = 180°$ to have a narrower and shorter wake than the baseline and strut only cases. Therefore, positioning the torque arms upstream of the strut acts to interrupt shedding from the strut with the resulting wake having a smaller momentum deficit than the strut only case.

2. On-Surface Pressure Fluctuations and Noise Sources

On-surface pressures are plotted for the three microphones in Figure 12. Microphone 1 shows that the strut only case records a weak peak at $St = 0.5$ which corresponds to shedding at 0.25 due to the microphone laying along the drag dipole. The shedding peak is suppressed by affixing torque arms at $\phi = 0°$, as highlighted

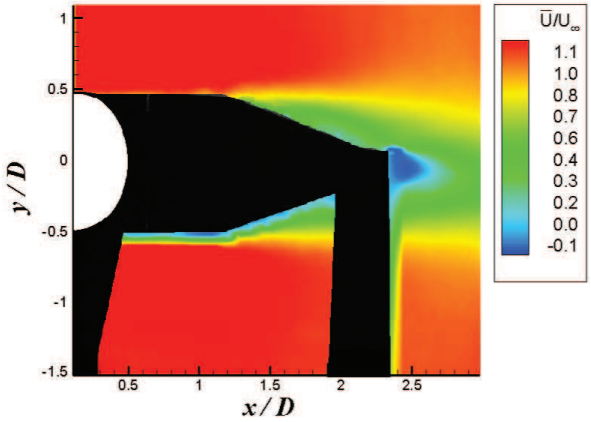

(a) Strut with torque arms, $\phi = 0°$.

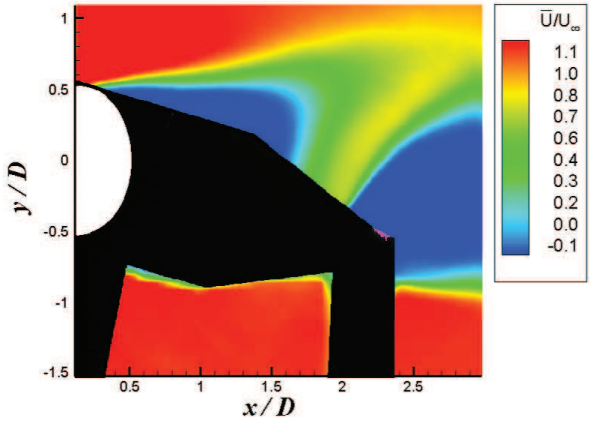

(b) Strut with torque arms, $\phi = 15°$.

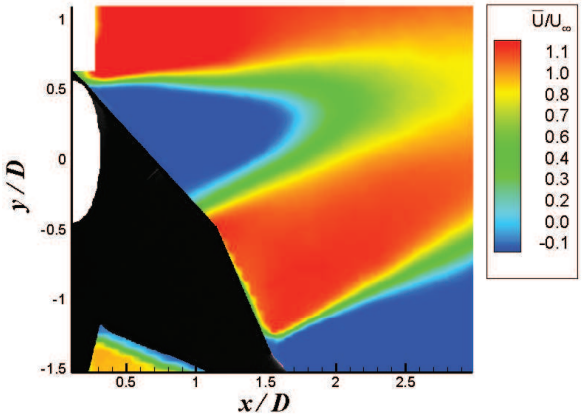

(c) Strut with torque arms, $\phi = 45°$.

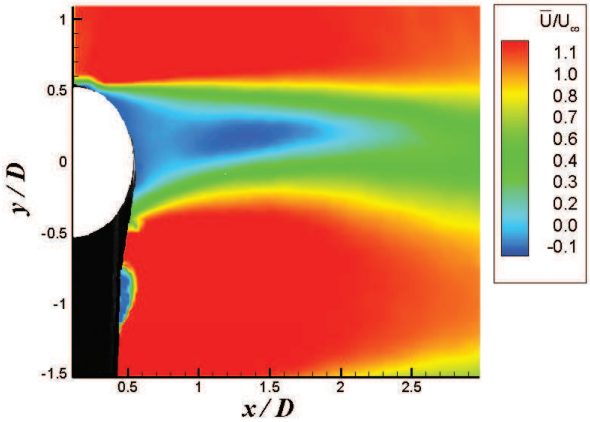

(d) Strut with torque arms, $\phi = 90°$.

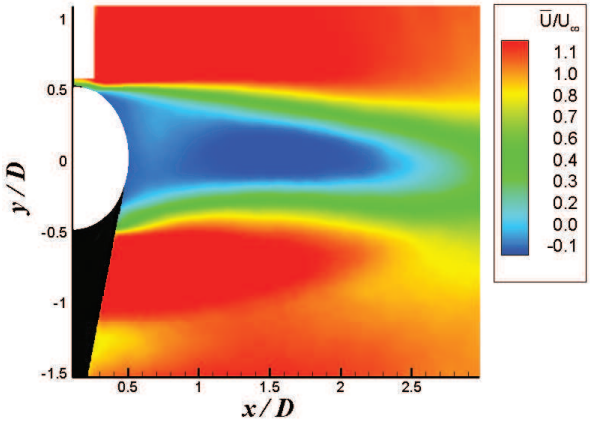

(e) Strut with torque arms, $\phi = 135°$.

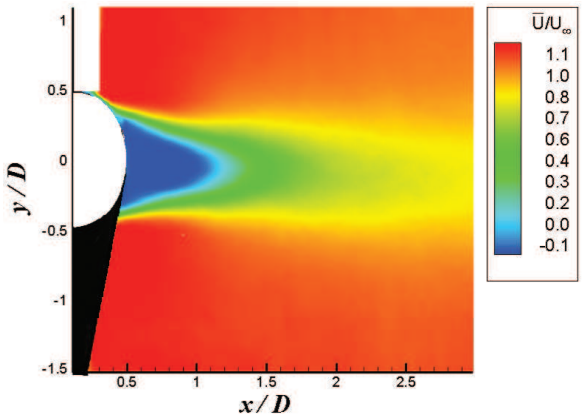

(f) Strut with torque arms, $\phi = 180°$.

Figure 9. Mean streamwise velocity for strut only and configurations with varying yaw angle, torque link angle $\theta = 90°$, $z/D = 4.5$.

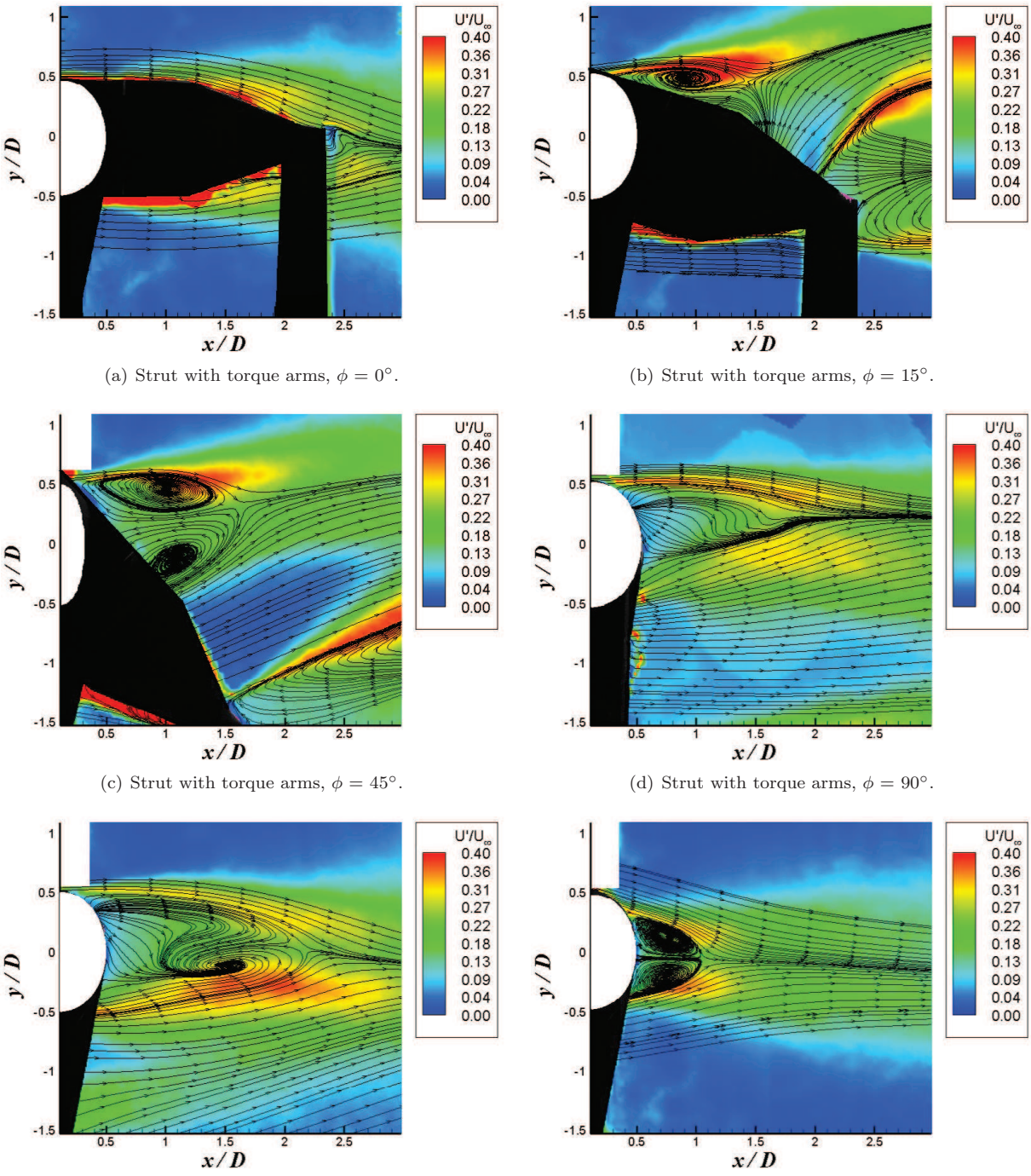

(a) Strut with torque arms, $\phi = 0°$.

(b) Strut with torque arms, $\phi = 15°$.

(c) Strut with torque arms, $\phi = 45°$.

(d) Strut with torque arms, $\phi = 90°$.

(e) Strut with torque arms, $\phi = 135°$.

(f) Strut with torque arms, $\phi = 180°$.

Figure 10. Root-mean-squared velocity with streamlines for strut only and configurations with varying yaw angle, torque link angle $\theta = 90°$, $z/D = 4.5$.

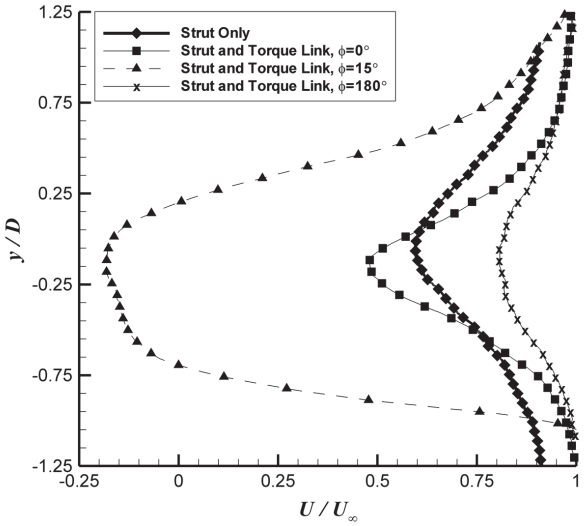

Figure 11. Wake profiles along $x/D = 2.7$ for strut only and configurations with varying yaw angle, torque link angle $\theta = 90°$.

by PIV mean streamlines in Figure 10 which showed lower velocity fluctuations behind the strut once the torque arms were attached. Furthermore, lower pressure levels are recorded across the whole St range. This result supports previously discussed behaviour. The cases for $15° \leq \phi \leq 45°$ show a tonal peak at $St = 0.25$ corresponding to periodic vortex shedding, this figure is not recorded at double the shedding frequency as the microphone does not lie on the drag dipole for these configurations. At $\phi = 90°$ the shedding peak is further reduced to $St = 0.2$, this reduction of the vortex shedding peak is due to separation occurring later on the surface of the strut with a resulting narrower wake. At $\phi = 90°$ there are two separate wakes, one emanating from the strut and one from the torque arm junction. The wake from the strut is much narrower than for $15° \leq \phi \leq 45°$ due to less interference from the torque arms. However, the shedding peak from $\phi = 90°$ is also smaller than the strut only, which suggests that having the torque arms extending into the freestream still acts to modify the flow from the strut. For yaw angles of $135° \leq \phi \leq 180°$ there is increased unsteadiness for $St \geq 1$, with a peak recorded at $St = 3$. At the torque arms are positioned upstream of the strut for these yaw angles, these fluctuations at increased Strouhal numbers may be caused by the wake from the torque arms impinging upon the strut. From $45° \leq \phi \leq 90°$ a broadband hump is present at high frequencies and becomes more exaggerated for increasing yaw angles. This hump is due to the microphone laying inside the turbulent boundary layer for these yaw angles. Microphone 3 shows no discernable peak at $St = 0.25$, due to the proximity of the torque arms to the strut acting to suppress vortex shedding.

Phased microphone plots were integrated over 2 kHz $\leq f \leq$ 8 kHz and plotted in the same manner as the previous investigation. The integrated SPL are presented in Figure 13(a) and show the baseline case to be the third loudest configuration over the 2 kHz $\leq f \leq$ 8 kHz frequency range. Yaw angles $\phi = 150°$ and 180° record higher local noise levels, as at these yaw angles the torque arms are positioned upstream of the strut, either completely or almost aligned with the strut. Therefore, the resulting interaction noise is louder than the baseline case of $\phi = 0°$. This is due to the torque arms not shielding the strut as effectively as the baseline case where the strut completely shields the torque arms. Due to the shape of the torque arms, i.e. they taper in towards the torque arm junction, when they are positioned upstream, not only is the frontal area of the torque arms exposed to the freestream but also parts of the strut are exposed to the freestream. Therefore, there is increased interaction between the components than the baseline case, leading to the measured increase in local noise levels. The quietest local noise levels over 2 kHz $\leq f \leq$ 8 kHz are recorded for $\phi = 75°$ and 90° as these configurations feature little or no interaction noise.

The SPL are plotted over the frequency range in Figure 13(b). At 2 kHz the configurations lie in two distinct groups, $\phi = 0°$, 15° and 180° record local noise levels approximately 2 dB higher than yaw angles of $45° \leq \phi \leq 135°$. This is due to the torque arms being either completely aligned with the strut ($\phi =$

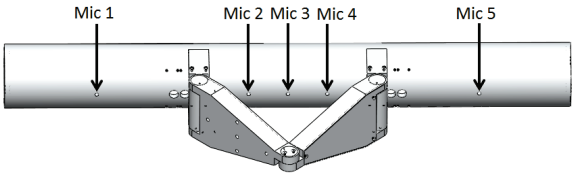

(a) Microphone locations.

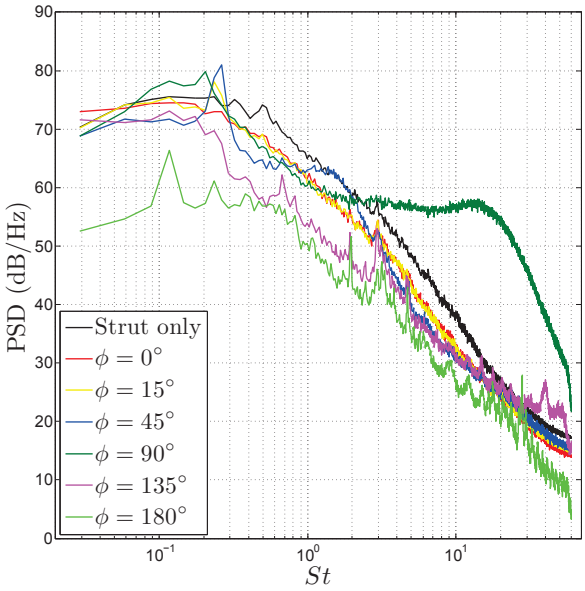

(b) Microphone 1.

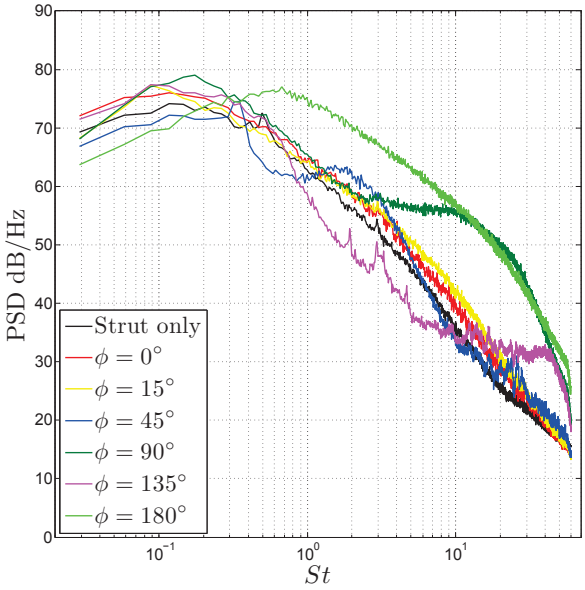

(c) Microphone 2.

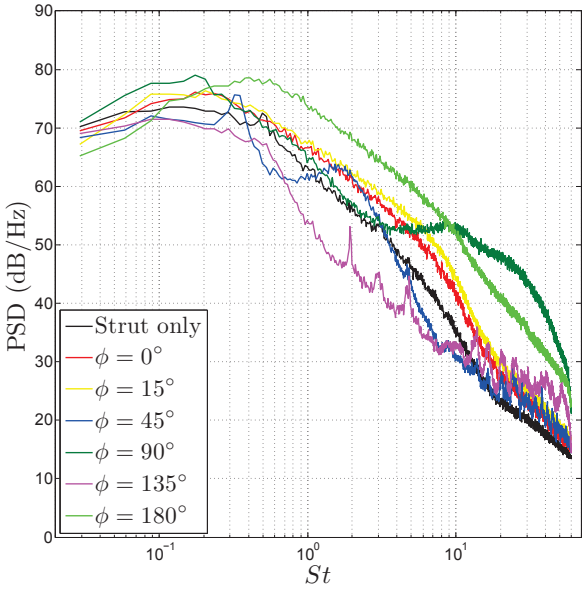

(d) Microphone 3.

Figure 12. PSD for varying yaw angle.

0° and 180°) or just out of alignment ($\phi = 15°$). Therefore, these configurations feature a higher level of interaction noise. For yaw angles of $45° \leq \phi \leq 135°$ the torque arms extend further into the freestream, with the maximum at $\phi = 90°$, therefore by recording lower levels at 2 kHz it is shown that any additional noise caused by the torque arms extending into the freestream is less than interaction noise. This phenomenon dissipates at higher frequencies, at 4 kHz $\phi = 45°$ records a higher local noise level than the baseline case. This is because $\phi = 45°$ features the greatest frontal area in contact with the freestream, therefore at this frequency additional noise sources are louder than the interaction noise recorded at $\phi = 0°$.

The lowest local noise level over the 2 kHz $\leq f \leq$ 8 kHz frequency range is recorded for $\phi = 90°$ as this configuration features no interaction of flow between components and thus no interaction noise. The loudest configuration is $\phi = 180°$ which confirms that despite showing favourable aerodynamic measurements such as increased drag and lower momentum deficit than the baseline case, aeroacoustic measurements show $\phi = 180°$ to generate more noise than all other configurations in the frequency range tested.

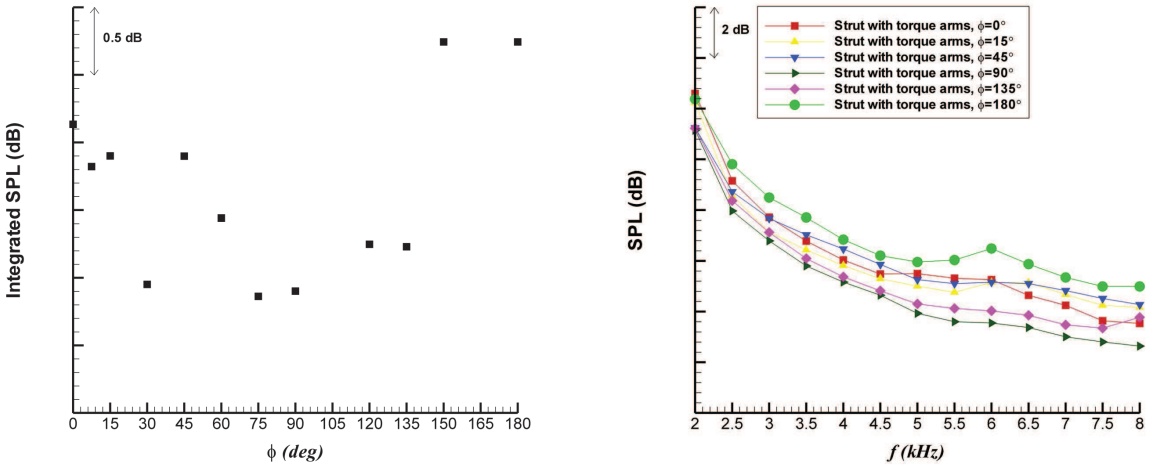

(a) Integrated SPL (dB).

(b) SPL (dB).

Figure 13. Beamforming maps integrated over 2 kHz $\leq f \leq$ 8 kHz for varying yaw angles, torque link angle θ = 90°.

IV. Conclusions

Aerodynamic and aeroacoustic measurements were performed on a generic torque link model. The torque link angle and yaw angle were varied in order to determine the optimal angles for decreased noise levels and future noise attenuation methods. Varying the torque link angle was shown to affect whether the strut and torque arms behaved as a single bluff body with decreased drag and suppression of shedding from the strut, or as two separate bluff bodies. PIV and wake profiles confirmed that $\theta = 130°$ yielded the lowest momentum deficit with a faster recovery to the freestream than all other torque link angles. However, phased microphone array measurements found no discernable decrease in local noise levels for varying torque link angle in the frequency range tested. Therefore, this investigation shows that finding favourable results in aerodynamic measurements cannot guarantee favourable acoustic results. Hence, aerodynamic and aeroacoustic measurements must be conducting in tandem in order to assess airframe noise.

Varying the yaw angle from the baseline case of $\phi = 0°$ was shown to yield several different flow regimes. Periodic shedding was shown to be suppressed for yaw angles of $90° \leq \phi \leq 135°$. At lower frequencies interaction noise was shown to dominate any additional noise caused by extending the torque arms into the freestream. This phenomenon was shown to decrease at higher frequencies, with $\phi = 45°$ recording higher levels than the baseline case. However, as lower frequencies translate to increased farfield noise levels, yaw angles such as $\phi = 90°$ with lower local noise levels may record lower farfield noise levels. The lowest local noise levels over 2 kHz $\leq f \leq$ 8 kHz were recorded for $\phi = 90°$. Whereas $\phi = 180°$ was shown to be louder than all other configurations due to higher levels of interaction noise. A yaw angle of $\phi = 90°$ is considered

optimal as it recorded both favourable aerodynamic and aeroacoustic measurements including suppressed vortex shedding, decreased local noise levels and drag levels 72% higher than the baseline case.

Acknowledgments

The funding for this research project was provided by EADS Innovation Works UK. The authors would like to thank David Cardwell and David Marshall for their help during the experiments.

References

[1]Watson, M. and Lambert, C., "ACARE Explained," *SBAC Aviation and Environment Briefing Papers*, Vol. 6, 2008.

[2]Heller, H. H. and Dobrzynski, W. M., "Sound Radiation from Aircraft Wheel-Well / Landing-Gear Configurations," *Journal of Aircraft*, Vol. 14, No. 8, 1977, pp. 768–774.

[3]Souliez, F. J., Long, L. N., Morris, P. J., and Sharma, A., "Landing Gear Aerodynamic Noise Prediction using Unstructured Grids," *International Journal of Aeroacoustics*, Vol. 1, No. 2, 2002, pp. 115–135.

[4]Dobrzynski, W., Chow, L. C., Guion, P., and Shiells, D., "A European Study on Landing Gear Airframe Noise Sources," *6th AIAA/CEAS Aeroacoustics Conference*, AIAA 2000-1971, Lahaina, Hawaii, 12 - 14 June 2000.

[5]Khorrami, M. R., Choudhari, M. M., Lockard, D. P., Jenkins, L. N., and McGinley, C. B., "Unsteady Flowfield Around Tandem Cylinders as Prototype Component Interaction in Airframe Noise," *AIAA Journal*, Vol. 45, No. 8, 2007, pp. 1930 – 1941.

[6]Jaeger, S. M., Soderman, P. T., Horne, W. C., and James, K. D., "Microphone Array Assessment of an Isolated, 26% Scale, High Fidelity Landing Gear," *8th AIAA/CEAS Aeroacoustics Conference*, AIAA 2002-2410, Breckenridge, Colorado, 17 - 19 June 2002.

[7]Huang, X. and Zhang, X., "Plasma Actuators for Noise Control," *International Journal of Aeroacoustics*, Vol. 9, No. 4, 2010, pp. 679–704.

[8]Huang, X., Zhang, X., and Li, Y., "Broadband Flow Induced Sound Control using Plasma Actuators," *Journal of Sound and Vibration*, Vol. 329, 2010, pp. 2477–2489.

[9]Huang, X., Zhang, X., and Gabriel, S., "Bluff Body Noise and Flow Control with Atmospheric Plasma Actuators," *14th AIAA/CEAS Aeroacoustics Conference*, AIAA 2008-3044, Vancouver, Canada, 5 - 7 May 2008.

[10]Ravetta, P. A., Burdisso, R. A., and Ng, W. F., "Wind Tunnel Aeroacoustic Measurements of a 26%-scale 777 Main Landing Gear Model," *10th AIAA/CEAS Aeroacoustics Conference*, AIAA 2004-2885, Manchester, Great Britain, 10 - 12 May 2004.

[11]Guo, Y., "A Statistical Model for Landing Gear Noise Prediction," *Journal of Sound and Vibration*, Vol. 282, 2005, pp. 61 – 87.

[12]Guo, Y. P., Stoker, R. W., and Yamamoto, K. J., "Experimental Study on Aircraft Landing Gear Noise," *Journal of Aircraft*, Vol. 43, No. 2, 2006, pp. 306–317.

[13]Dobrzynski, W. M., Schoning, B., Chow, L., Wood, C., Smith, M., and Seror, C., "Design and Testing of Low Noise Landing Gears," *International Journal of Aeroacoustics*, Vol. 5, No. 3, 2006, pp. 233–262.

[14]Zawodny, N. S., Liu, F., Yardibi, T., Cattafesta, L., Khorrami, M. R., Neuhart, D. H., and Van De Ven, T., "A Comparative Study of a 1/4 - Scale Gulfstream G550 Aircraft Nose Gear Model," *15th AIAA/CEAS Aeroacoustics Conference (30th AIAA Aeroacoustics Conference)*, AIAA 2009-3153, Miami, Florida, 11-13 May 2009.

[15]Neuhart, D., Khorrami, M., and Choudhari, M., "Aerodynamics of a Gulfstream G550 Nose Landing Gear Model," *15th AIAA/CEAS Aeroacoustics Conference (30th AIAA Aeroacoustics Conference)*, AIAA 2009-3152, Miami, Florida, 11-13 May 2009.

[16]Igarashi, T., "Characteristics of the Flow Around Two Circular Cylinders Arranged in Tandem," *Japan Society Mechanical Engineering Bulletin*, Vol. 24, 1981, pp. 323–331.

[17]Zdravkovich, M., *Flow around circular cylinders: Vol 1*, Oxford University Press, 1997.

[18]Castro, I. P., "Hot Wire Anemometry with the Newcastle, NSW Bridges," Tech. rep., 2001.

[19]Fenech, B. A. and Takeda, K., "SotonArray : Southampton University Wind Tunnel Microphone Array System Guide," *AFM Technical Report*, , No. 3, 2007, pp. 1 – 33.

[20]Shih, W., Wang, C., Coles, D., and Roshko, A., "Experiments on Flow Past Rough Circular Cylinders at Large Reynolds Numbers," *Journal of Wind Engineering and Industrial Aerodynamics*, Vol. 49, 1993, pp. 351–368.

[21]Achenbach, E., "Influence of Surface Roughness on the Cross-Flow Around a Circular Cylinder," *Journal of Fluid Mechanics*, Vol. 46, No. 2, 1971, pp. 321 – 335.